Uluslararası Teknolojik Bilimler Dergisi
International Journal of Technological Sciences
UTBD
IJTS

Araştırma Makalesi/Research Article

ÇBAG Tabanlı rüzgar türbinleri için yeni bir düşük gerilim iyileştirme yeteneği stratejisi

M. Kenan Döşoğlu *[1]

[1]Düzce Üniversitesi, Teknoloji Fakültesi, Elektrik Elektronik Mühendisliği Bölümü, 81620, Düzce, Türkiye

Anahtar Kelimeler
ÇBAG
Pozitif dizi modeli
Negatif dizi modeli
Doğal güçlendirilmiş akı modelleri
Stator-rotor EMK

Makale geçmişi:
Geliş Tarihi: 10.01.2020
Kabul Tarihi: 20.04.2020

Özet: Çift beslemeli asenkron generatör (ÇBAG) tabanlı rüzgar türbinlerinde gerilim düşümü sorunlarının üstesinden gelmek için kullanılan başlıca yöntemlerden biri düşük gerilim iyileştirme (DGİ) yeteneğidir. Simetrik ve asimetrik arızalar sırasında bu tür gerilim düşüm problemlerini çözmek için, bu çalışmada ÇBAG'de DGİ yeteneğ için yeni bir geliştirilmiş dinamik modelleme yaklaşımı sunulmuştur. Pozitif ve negatif dizi modelleri, doğal ve güçlendirilmiş akı modelleri ile birlikte bir ÇBAG için önerilen DGİ yeteneği stratejisi kullanılmıştır. Ayrıca, stator ve rotor devre modelinin geliştirilmesi için elektro-motor kuvveti (EMK) uygulanmıştır. Yeni stator-rotor dinamik modellemesi, üç faz ve iki faz arızalara karşı geçici kararlılık çalışmasını iyileştirmek içinde kullanılmıştır. Amaçlanan dinamik modellemenin uygulanmasında, sistemin kısa bir süre içinde kararlı hale gelmiş ve salınımlar sönümlenmiştir.

Atıf için/To Cite: Döşoğlu MK. ÇBAG Tabanlı rüzgar türbinleri için yeni bir düşük gerilim iyileştirme yeteneği stratejisi. Uluslararası Teknolojik Bilimler Dergisi, 12(1), 45-55, 2020.

A novel low voltage ride through capability strategy for DFIG based wind turbines

Keywords
DFIG
Positive sequence model
Negative sequence model
Natural-forcing flux models
Stator-rotor EMF

Article history:
Received: 10.01.2020
Accepted: 20.04.2020

Abstract: One of the chief methods used to overcome voltage dip problems in doubly fed induction generator (DFIG)-based wind turbines is low voltage ride through (LVRT) capability. In order to solve such voltage dip problems during symmetrical and asymmetrical grid faults, this study presents a novel enhanced dynamic modeling approach for LVRT in DFIG. Positive and negative sequence models, along with natural and forcing flux models were used to enhance the proposed LVRT capability strategy for a DFIG. In addition, electro-motor-force (EMF) was applied for the enhancement of the stator and rotor circuit model. The novel stator-rotor dynamic modeling was also used in boosting the transient stability operation against three phase and two phase faults. When the proposed dynamic modeling was applied, the system was stabilized within a short amount of time and the oscillations ceased.

1. Introduction

With today's increasing load demands, there are a number of methods that can be used to improve power system operating conditions. The connection of the systems with wind turbines is among the most promising of these approaches. However, in order to maintain system stability as the wind power increasingly penetrates the system, the wind turbines must stay connected to the power grid. When a voltage dip occurs, the use of a DFIG with the wind turbine can successfully control the system active power and torque and thus enhance the LVRT capability during various grid fault events. The following are the most commonly used of the various control model techniques for LVRT capability in DFIG mentioned in the literature. In the event of balanced or unbalanced faults, LVRT capability in DFIG is essential to counteract voltage dips by providing voltage support. Consequently, a vector control model has been used to improve LVRT capability in DFIG [1],[2]. In addition to vector control, DC link dynamic control, designed to protect the converter against over-voltage and over-current during faults, has also been successfully used for this purpose [3],[4]. A control strategy dependent on the positive and negative sequences model and

* M.Kenan Döşoğlu:kenandosoglu@duzce.edu.tr

augmented with current reference values was proposed for torque control during unbalanced voltage dips [5]. Supplementary rotor current control and series dynamic braking resistor models were used in DFIG to protect the Rotor Side Converter (RSC) and Grid Side Converter (GSC) [6],[7]. In order to co-ordinate RSC and GSC control of the DFIG together with the grid voltage during balanced and unbalanced faults in a DFIG, a voltage control strategy was developed [8]. Rotor voltage control is dependent on the rotor terminal voltage with controllable limits. The rotor voltage control was enhanced in order to determine the dynamic behavior of a DFIG. Thus, through this control strategy, the LVRT capability was ensured [9]. Moreover, a passive-impedance model was used to support the LVRT capability of a DFIG during both balanced and unbalanced voltage dips and series. These models were effective in achieving high efficiency operation at low cost for manufacturing and for maintenance as well [10],[11]. Another approach developed for LVRT capability in DFIG is that of series voltage compensation, in which a series compensator is added to the GSC for its utilization. By providing a series compensator, this technique delivers voltage injection to the line as a series [12]. In a DFIG, a proposed LVRT method employing a dynamic control strategy was applied to both the RSC and the GSC. Furthermore, a feed-forward was utilized to attain transient stability in the DFIG [13],[14]. Dynamic modeling using a base voltage source was designed for both stator and rotor circuit LVRT in the DFIG. In addition, reference current controllers were enhanced for the transient stability of the DFIG [15]-[17]. There are a number of methods being used to control the in DFIG for LVRT capability fault detection. The steady-state and transient components of the stator quantities are applied in the most commonly used methods [18]. Included in these stator components are voltage, current and power for the detection of turn faults, broken rotor bars, bearing failures and air gaps [19],[20]. During different faults, different strategies have been applied for the enhancement of series and parallel compensators, which are referred to as FACTS devices. These devices are important for LVRT capability in DFIG [21]-[24] and due to the proposed LVRT control strategy, they enable control of the RSC and GSC in the event of balanced and unbalanced voltage dips. Moreover, the proposed control strategy provides for the enhancement of new flux and rotor electromotive force models [25]-[29]. Demagnetizing current control and natural flux models were enhanced in the system and its dynamic behaviors were investigated during voltage sags in the DFIG [30],[31]. Active and passive compensators were used to enhance LVRT capability in a DFIG. The active compensator used the rotor reference current for over-voltage during voltage dips, while the passive compensator used the rotor current limiter for inrush current during voltage dips [32],[33]. Furthermore, the RSC is able to restrict the stator-rotor inrush current, whereas the GSC has the ability to supply reactive power to support the grid, thereby ensuring recovery of the voltage in the grid. The passive compensator draws upon the fact that a rotor current limiter resistor is present in series with the rotor windings [34]. This study developed a dynamic model for rotor circuit LVRT capability in a DFIG. In addition, a novel capability method for LVRT was enhanced with models for stator and rotor electro-motor-force (EMF), and positive and negative sequences and natural and forcing models for various balanced and unbalanced faults. Positive and negative sequence models and natural flux were used as references [34]. In addition to positive and negative sequence models, this study also used natural, forcing component, stator and rotor EMF models for the test system. Moreover, the study investigated 34.5 kV bus voltage, terminal voltage, angular speed, electrical torque and d-q axis stator current variations. The findings of this study demonstrated that the enhanced stator-rotor dynamic models were effective against symmetrical and asymmetrical faults.

2. Modeling of DFIG

The DFIG components consist of a wound-rotor induction generator with the stator windings connected directly to the three-phase network and the rotor windings connected to a back to back. The DFIG is comprised of a RSC and GSC connected to a common DC bus and crowbar unit. Figure 1 illustrates the DFIG circuit model.

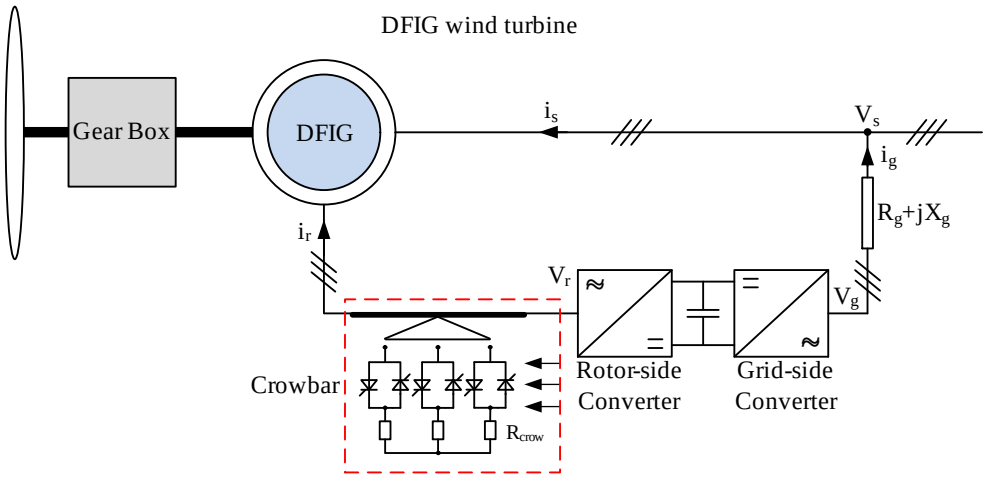

Figure 1. DFIG modeling

The DFIG stator winding is connected to the grid, while the motor winding is connected to the back-to-back converter unit. Both converters play important roles in controlling magnitude and angle and DFIG active-reactive power during steady and transient states. The calculations for the DFIG active-reactive powers are shown in Equations (1) and (2).

$$P_s = V_{grid}\frac{L_m}{L_s} i_{dqr} \tag{1}$$

$$Q_s = V_{grid}\frac{L_m}{L_s} i_{dqr} - \frac{V_{grid}^2}{w_s L_s} \tag{2}$$

When the variables of the generator within the d–q synchronous reference frame were considered, four equations were used to represent the DFIG model. Equations (3)-(6) were used for the stator and rotor windings.

$$v_{ds} = R_s i_{ds} + jw_s\lambda_{qs} + \frac{d}{dt}\lambda_{ds} \tag{3}$$

$$v_{qs} = R_s i_{qs} - jw_s\lambda_{ds} + \frac{d}{dt}\lambda_{qs} \tag{4}$$

$$v_{dr} = R_r i_{dr} - jsw_s\lambda_{qr} + \frac{d}{dt}\lambda_{dr} \tag{5}$$

$$v_{qr} = R_r i_{qr} + jsw_s\lambda_{dr} + \frac{d}{dt}\lambda_{qr} \tag{6}$$

The d–q coordinates are given in the flux-inductance equations that follow.

$$\lambda_{ds} = \left(L_s + L_m\right) i_{ds} + L_m i_{dr} \tag{7}$$

$$\lambda_{qs} = \left(L_s + L_m\right) i_{qs} + L_m i_{qr} \tag{8}$$

$$\lambda_{dr} = \left(L_r + L_m\right) i_{dr} + L_m i_{ds} \tag{9}$$

$$\lambda_{qr} = \left(L_s + L_m\right) i_{qr} + L_m i_{qs} \tag{10}$$

Where, v_{ds}, v_{dr}, v_{qs}, v_{qr} are the d and q axis voltages of the stator and rotor; i_{ds}, i_{dr}, i_{qs}, i_{qr} are the d and q axis currents of the stator and rotor; λ_{ds}, λ_{qs}, λ_{dr}, λ_{qr} are the d and q axis fluxes of the stator and rotor; w_s is the angular speed of the stator; s is the slip; R_s and R_r are the stator and rotor resistance; L_s and L_r are the stator and rotor inductance; L_m is the magnetic inductance [35]-[38].

3. Enhancement of Dynamic Modeling in DFIG

Stator dynamic of the DFIG model is used to ease computation for symmetrical and unsymmetrical faults. In stator EMF model, a stator is formed through a transient voltage source and transient reactance where stator fluxes derivation is neglected. In this study, the main propose is that the DC element is archived by the stator transient current [28],[29]. Related equations about stator dynamic are given in (11)-(17) as follows:

$$v_{ds} = R_s i_{ds} - X' i_{qs} + e_{ds} \tag{11}$$

$$v_{qs} = R_s i_{qs} + X' i_{ds} - e_{qs} \tag{12}$$

$$\frac{de_{ds}}{dt} = -\frac{1}{T_0}\left[e_{ds} - \left(X - X^{'}\right)\times I_{qs}\right] + s\times w_s \times e_{qs} - w_s \times \frac{L_m}{L_m + L_s}\times v_{dr} \quad (13)$$

$$\frac{de_{qs}}{dt} = -\frac{1}{T_0}\left[e_{qs} + \left(X - X^{'}\right)\times I_{ds}\right] - s\times w_s \times e_{ds} + w_s \times \frac{L_m}{L_m + L_s}\times v_{qr} \quad (14)$$

$$M = e_{ds} i_{qs} + e_{qs} i_{ds} \quad (15)$$

$$X^{'} = w_s \left(\left(L_m + L_s\right) - \frac{L_m^2}{L_m + L_r} \right) \quad (16)$$

$$T_0 = \frac{L_r + L_m}{R_r} \quad (17)$$

where, e_{ds} and e_{qs} : d axis and q axis source voltages of stator, X: stator reactance, X′ transient reactance, and M :torque. T_0: transient open circuit time constant [37]. Stator voltage in stator dynamic model, two components can be activated when faults occur. These are described as positive and negative sequence stator voltages, as seen in Equation (18).

$$v_{dqs} = V_{s1} e^{jw_s t} + V_{s2} e^{-jw_s t} \quad (18)$$

When symmetrical grid faults are present, the negative sequence model in Equation (18) is zero. Small voltage dips were not taken into account in the stator resistance in Equations (11), (12) and (18). The steady-state components of the stator flux during grid faults are shown in Equation (19).

$$\lambda_{ss} = \lambda_{s1} + \lambda_{s2} = \frac{V_{s1}}{jw_s} e^{jw_s t} + \frac{V_{s1}}{-jw_s} e^{-jw_s t} \quad (19)$$

With improved dynamic stability in DFIG, the principle of constant flux linkages asserts that the stator flux cannot track stator voltage instantaneous changes and natural-forcing components created within it, in order to guarantee continuity of the stator flux during grid faults. Therefore, the total stator flux incorporates the steady and state components and the natural and forcing components: Equation (20) gives the calculations for the steady and state components and the natural and forcing components in the stator flux.

$$\lambda_{dqs} = \lambda_{s1} + \lambda_{s2} + \lambda_{sn} + \lambda_{nf} = \frac{V_{s1}}{jw_s} e^{jw_s t} + \frac{V_{s1}}{-jw_s} e^{-jw_s t} + \left(\lambda_{sn0} + \lambda_{nf0}^{\ -t/\tau_s}\right) e^{-t/\tau_s} \quad (20)$$

The stator flux positive sequence emerges with a counterclockwise rotation of the space vectors at slip speed s. w_s in the rotor reference frame, as seen in Equation (21).

$$\lambda_{dqr} = \left(\lambda_{sn0} + \lambda_{nf0}\right) e^{-t/\tau_s} e^{jwt} + \frac{V_{s1}}{jw_s} e^{js.w_s t} + \frac{V_{s1}}{-jw_s} e^{-j(2-s)w_s t} \quad (21)$$

However, the stator flux negative sequence and natural and forcing components emerge with the clockwise rotation of the space vectors at (2-s) w_s and w_m speed, respectively. Therefore, the use of the rotor dynamic model depending on rotor voltage is preferred. The components of the rotor voltage can be demonstrated as follows:

$$v_{r1} = R_r i_{dqr1} + \sigma L_r \frac{di_{dqr1}}{dt} + \frac{L_m}{L_s} s + V_{s1} e^{jw_s t} \quad (22)$$

$$v_{r2} = R_r i_{dqr2} + \sigma L_r \frac{di_{dqr2}}{dt} + \frac{L_m}{L_s}\left(2 - s\right) + V_{s2} e^{-j(2-s)w_s t} \quad (23)$$

$$v_{rn} = R_r i_{rn} + \sigma L_r \frac{di_{rn}}{dt} - \frac{L_m}{L_s}\left[\left(\frac{1}{\tau_s} + jw_m \right)\left(\lambda_{sn0} + \lambda_{nf0}\right) e^{-t/\tau_s} e^{-jwt} \right] \quad (24)$$

In Equations (22), (23) and (24), the component in the rotor EMF voltage is triggered by the stator flux components and can be expressed as follows.

$$E_r = \frac{L_m}{L_s} s V_{s1} e^{js.w_s t} + \left(2 - s\right) V_{s2} e^{-j(2-s)w_s t} - \left[\left(\frac{1}{\tau_s} + jw \right)\left(\lambda_{sn0} + \lambda_{nf0}\right) e^{-t/\tau_s} e^{-jwt} \right] \quad (25)$$

The new LVRT strategy can be obtained by determining the rotor current references that reduce the rotor over-voltages during grid faults. Without considering

insignificant rotor resistance voltage dips, the rotor current tacking derivative, the negative sequence and the natural and forcing components of the rotor voltage can be expressed in Equations (23), (24) and (25) as follows:

$$v_{r2} = -j\left(2-s\right)w_s \sigma L_r i_{dqr2} + \frac{L_m}{L_s}\left(2-s\right) + V_{s2}e^{-j\left(2-s\right)w_s t} \quad (26)$$

$$v_{rn} = \left(\frac{1}{\tau_s} + jw_m\right)\sigma L_r - \frac{L_m}{L_s}\left[\left(\frac{1}{\tau_s} + jw_m\right)\left(\lambda_{sn0} + \lambda_{nf0}\right)e^{-t/\tau_s}e^{-jwt}\right] \quad (27)$$

The expected rotor voltage components are shown in Equations (28), (29) and (30). The rotor over-voltages during grid faults are reduced as seen in Equation (30) by injecting the rotor currents against the negative sequence and natural components of the stator flux and consequently reducing the rotor over-currents and DC-link over-voltage.

$$v_{r2} = -M_d \lambda_{s2} \quad (28)$$

$$v_{rn} = -\left(M_d \lambda_{sn} + M_d \lambda_{nf}\right) \quad (29)$$

$$i_{dqr} = -\left(M_d \lambda_{s2} + M_d \lambda_{sn} + M_d \lambda_{nf}\right) \quad (30)$$

Figure 2 presents a block diagram of the amplified sequence models for LVRT capability.

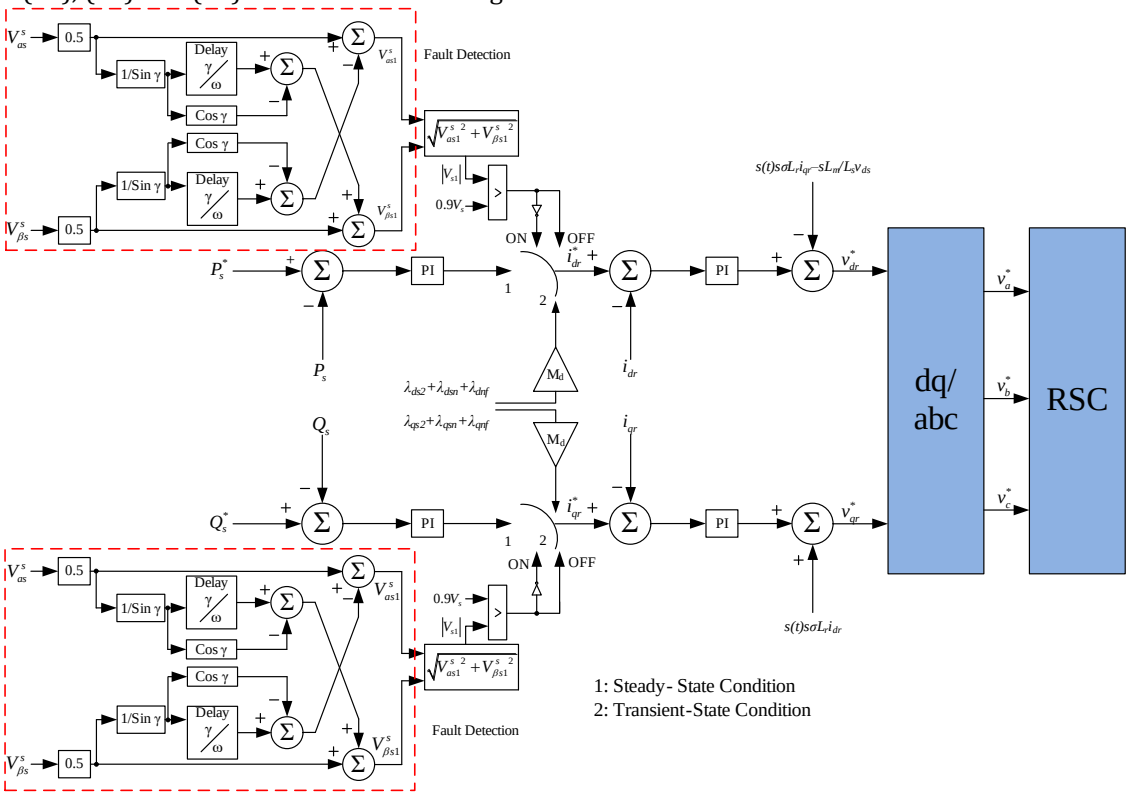

Figure 2. Block diagram of the stator-rotor dynamic model enhanced for LVRT capability

With conventional control methods, the rotor current references are computed to produce stator active and reactive powers while in a steady state. During a transient state, however, in order to utilize the maximum capacity of the RSC to improve LVRT capability, the power controller terminals were disconnected and the proposed control method was applied to determine the rotor current references directly. In the course of steady-state operation, the DC-link voltage control and reactive power control in the grid are provided by the GSC. In order to reduce the over-currents and losses in the RSC and GSC of the DFIG, the GSC reactive power reference was set to zero during steady-state operations. However, in order to meet the grid code requirements during transient state situations, it was necessary to use reactive power injection. Thus, during grid faults, the GSC was compensated for maximum reactive power in this study. The influence of the rotor current references on stator flux dynamics are given by placing the stator current

and the obtained stator natural and forcing component dynamics found in Equations (7)–(8) into Equations (11)–(12). This operation is expressed in Equations (31), (32), (33) and (34).

$$\frac{d\lambda_{sn}}{dt} = -\frac{R_s}{L_s}\lambda_{sn} + \frac{R_s L_m}{L_s} i_{rn} \tag{31}$$

$$\frac{d\lambda_{nf}}{dt} = -\frac{R_s}{L_s}\lambda_{nf} + \frac{R_s L_m}{L_s} i_{rn} \tag{32}$$

$$\frac{d\lambda_{sn}}{dt} = -\frac{1}{\tau_d}\lambda_{sn} \tag{33}$$

$$\frac{d\lambda_{nf}}{dt} = -\frac{1}{\tau_d}\lambda_{nf} \tag{34}$$

A shortened version of the stator natural and forcing fluxes during grid faults is given as follows in Equations (35) and (36):

$$\lambda_{sn} = \lambda_{sn0} e^{-t/\tau_d} \tag{35}$$

$$\lambda_{nf} = \lambda_{nf0} e^{-t/\tau_d} \tag{36}$$

The new time constant (delay constant) of the stator natural flux and stator forcing flux in the presence of the grid faults can be given in the following way:

$$\tau_d = \frac{\tau_s}{1 + L_m M_d} \tag{37}$$

Where, τ_d is the new time constant. In Equation (37), considerable decreases can be observed in the stator natural and forcing flux time constants, whereas the stator flux damping exhibits a tendency to increase.

4. Simulation Study

Figure 3 shows the 1.5 MW wind power system used for the analysis of the transient behavior of the wind turbine grid interaction [39].

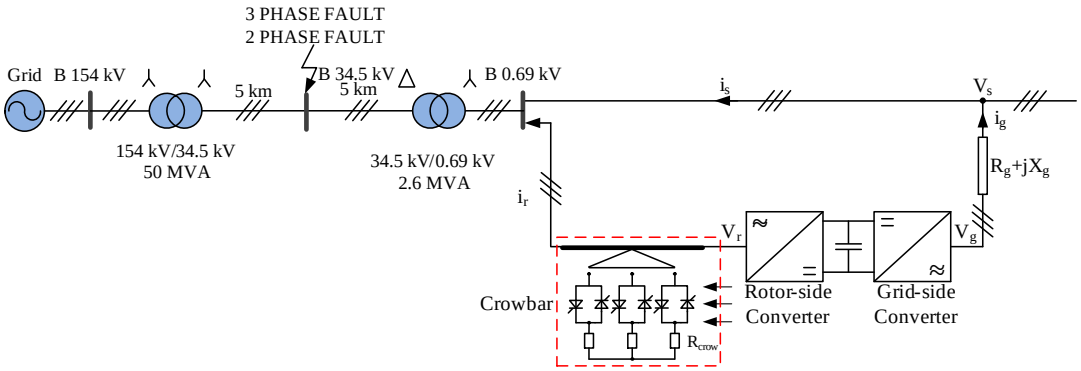

Figure 3. 1.5 MW wind power system [39]

This study performed stator-rotor dynamic modeling of the DFIG with a positive-negative sequence, natural-forcing components and stator-rotor EMF. Transformers having values of 50 MVA, 154 Y/34.5kV Y and 2.6 MVA, 34.5 Δ/0.69kV Y were used to connect the wind power plant to a 34.5 kV system. A 10-km distance was chosen from the plant to the 34.5 kV grids along with a constant wind speed of 8 m/s; 2500 MVA was determined as the 34.5 kV grid-side short circuit power and the X/R rate was established as 6. The generator parameters included a 0.00706-ohm stator resistance, 0.005-ohm rotor resistance, 0.171-Henry stator inductance, 0.156-Henry rotor inductance and 2.9-Henry magnetization inductance. In the simulation, 0.001 ohm and 10000 ohm were determined as the fault and snubber resistances, respectively. The time representation of the system and decomposition level approximations for defects in the inrush current collision demonstrated that the fault voltage drop could be obtained from the inrush current and the approximation of the decomposition levels that were generated. Moreover, fault detection was observed at t = 0.1 s.

5. Simulation Results

Two transient events disposed the effects of the positive-negative sequences, natural-forcing components and stator-rotor EMF on the system parameters. The first test transient event was a three phase fault created in a B 34.5 kV bus between 0.55 s and 0.6 s, with variations of 34.5 kV bus voltage,

terminal voltage, angular speed, electrical torque, and d-q axis stator current. These variations were designed for the case with and without the positive-negative sequences, natural-forcing components and stator-rotor EMF in figure 4.

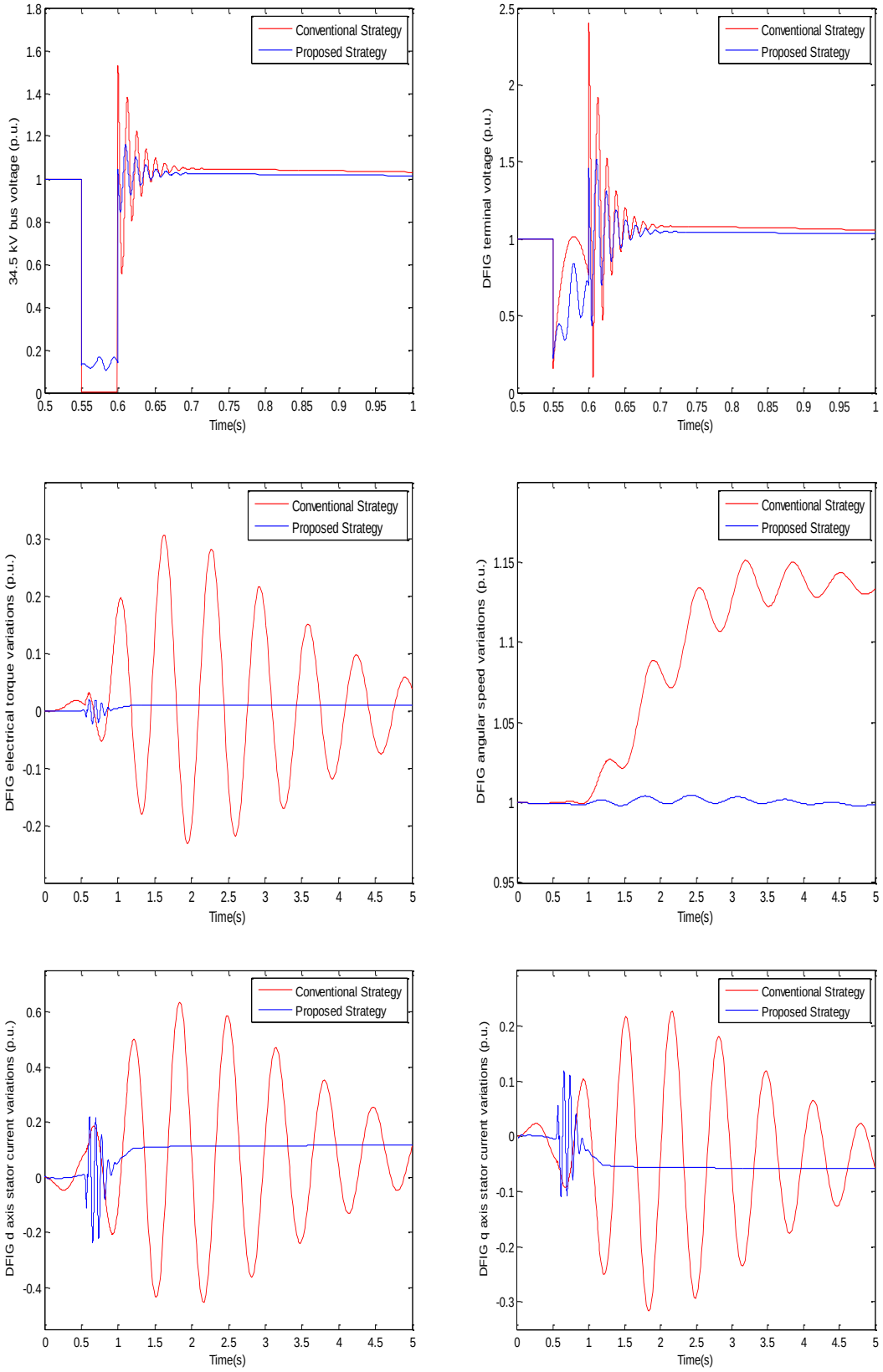

Figure 4. Test system simulation results in 3 phase fault

It can be seen in Figure 4 that the maximum values of 34 kV bus voltage and DFIG terminal voltage were decreased and the system was stabilized in a shorter period of time than with a conventional strategy using positive and negative sequence models, natural forcing flux models and stator-rotor EMF. With the novel approach presented in this study, the 34.5 kV bus voltages reached almost 0.175 p.u., in contrast with the conventional approach, which resulted in a value of 0 p.u. In addition, the use of the positive-negative sequence models natural-forcing flux models and stator-rotor EMF resulted in notable reductions in oscillations in angular speed and *d-q* axis stator currents.

For the second test transient event, a two phase fault was examined. Figure 5 shows (with and without the proposed strategy) the variations in 34 kV bus voltage, terminal voltage, electrical torque, angular speed and d-q axis stator current resulting from this two phase fault that emerged for between 0.55 and 0.6 s.

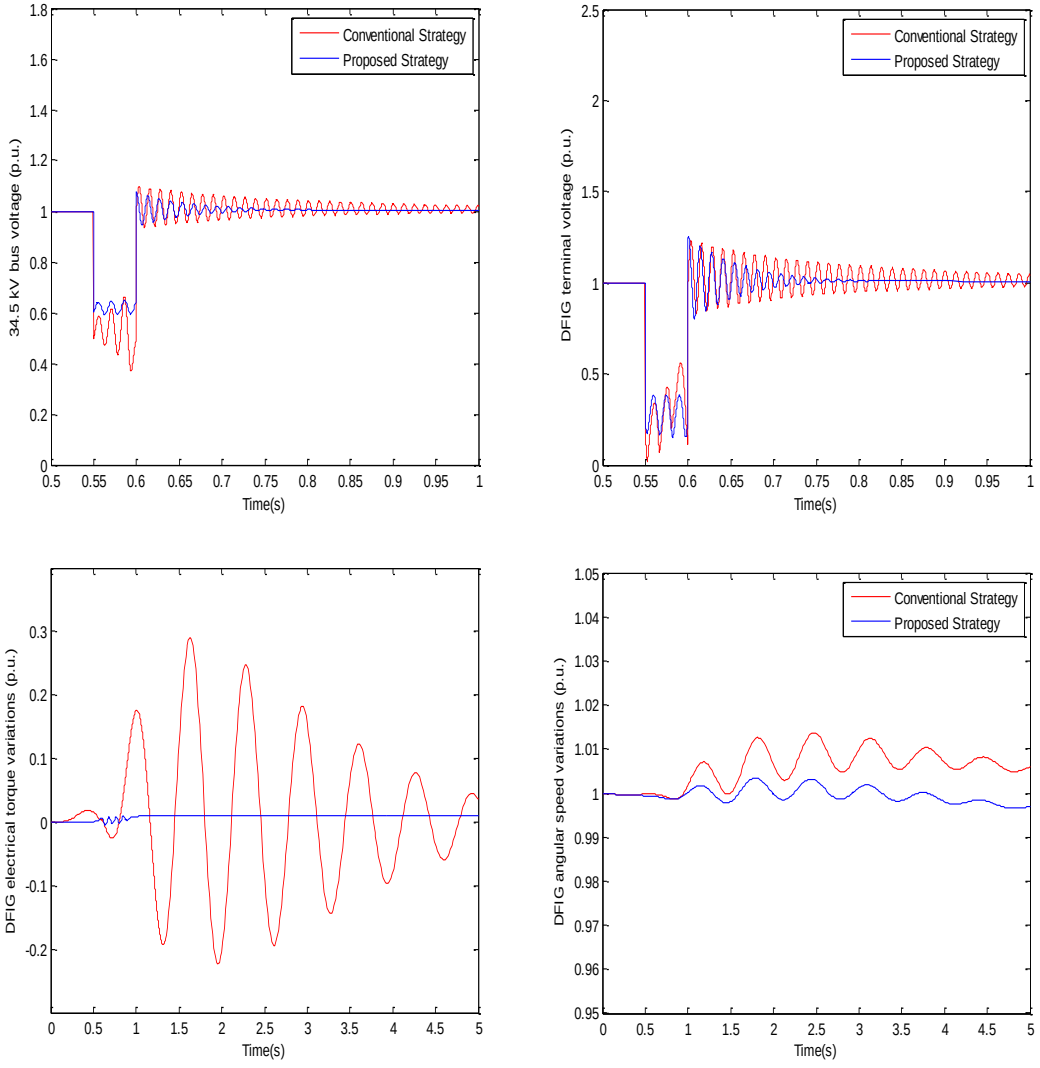

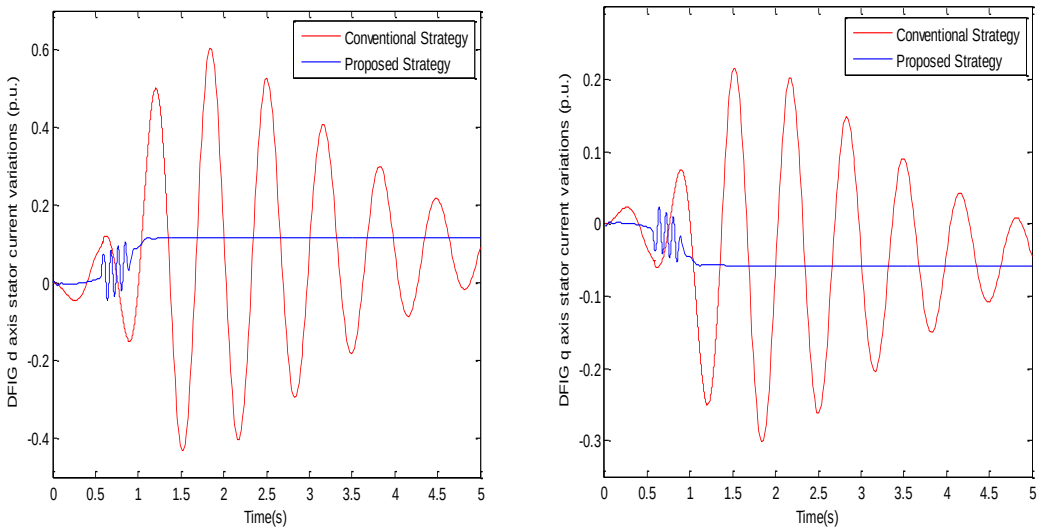

Figure 5. Test system simulation results in 2 phase fault

Maximum 34 kV bus voltage and DFIG terminal voltage values were decreased and the system was stabilized in a shorter duration than when the conventional strategy using positive-negative sequences, natural-forcing flux models and stator-rotor EMF were applied in Fig. 5. The novel approach presented in this study brought the 34.5 kV bus voltage to almost 0.6 p.u., while with the conventional approach the value achieved was 0.5 p.u. Furthermore, in this study, the proposed strategy resulted in notable reductions in oscillations in angular speed and d-q axis stator currents.

6. Conclusions

For DFIG, there are theoretical methods for RSC control against overvoltage and inrush current during balanced and unbalanced faults. This study presented a model for the enhancement of a grid-connected DFIG which was comprised of positive-negative sequences and natural-forcing components in addition to a stator-rotor EMF. The transient behaviors of the system with and without the proposed method were compared in terms of three phase and two phase faults. With the enhanced positive, negative sequences, natural-forcing components and stator-rotor EMF, the oscillations were lower during the three phase fault B 34.5 kV bus. The DFIG terminal voltage was increased when the enhanced approach was applied during varying faults. Findings of the simulation system analysis demonstrated that when the positive, negative sequences, natural forcing components and rotor EMF were connected to the DFIG, the oscillations that occurred following the transient events were controlled within a very short time.

References

[1] Chondrogiannis S, Barnes M. Specification of Rotor Side Voltage Source Inverter of A Doubly-Fed Induction Generator for Achieving Ride-Through Capability. *IET Renewable Power Generation*, 2(3), 139-150, 2008.

[2] Petersson A, Harnefors L, Thiringer T. Comparison between stator-flux and grid-flux-oriented rotor current control of doubly-fed induction generators. *In Power Electronics Specialists Conference, 2004. PESC 04*, Aachen, 20-25 June 2004.

[3] Dai J, Xu D, Wu B, Zargari NR. Unified DC-Link Current Control for Low-Voltage Ride-Through in Current-Source-Converter-Based Wind Energy Conversion Systems. *IEEE Transactions on Power Electronics*, 26(1), 288-297, 2010.

[4] Yang L, Xu Z, Ostergaard J, Dong ZY, Wong KP. Advanced Control Strategy of DFIG Wind Turbines for Power System Fault Ride Through. *IEEE Transactions on Power Systems*, 27(2), 713-722, 2012.

[5] Gomis-Bellmunt O, Junyent-Ferre A, Sumper A, Bergas-Jane J. Ride-Through Control of A Doubly Fed Induction Generator Under Unbalanced Voltage Sags. *IEEE Transactions on Energy Conversion*, 23, 4, 1036-1045, 2008.

[6] Okedu KE, Muyeen SM, Takahashi R, Tamura J. Wind Farms Fault Ride Through using DFIG with New Protection Scheme. *IEEE Transactions on Sustainable Energy*, 3(2), 242-254, 2012.

[7] Vidal J, Abad G, Arza J, Aurtenechea S. Single-Phase DC Crowbar Topologies for Low Voltage Ride Through Fulfillment of High-Power Doubly Fed Induction Generator-Based Wind Turbines. *IEEE Transactions on Energy Conversion*, 28(3), 768-781, 2013.

[8] Hansen AD, Michalke G, Sørensen P, Lund T, Iov F. Co-ordinated Voltage Control of DFIG Wind

Turbines In Uninterrupted Operation During Grid Faults. *Wind Energy*, 10(1), 51-68, 2007.

[9] Lima FK, Luna A, Rodriguez P, Watanabe EH, Blaabjerg F. Rotor Voltage Dynamics in The Doubly Fed Induction Generator During Grid Faults. *IEEE Transactions on Power Electronics*, 25(1), 118-130, 2010.

[10] Flannery, P. S., Venkataramanan, G., Unbalanced voltage sag ride-through of a doubly fed induction generator wind turbine with series grid-side converter, 2009, *IEEE Transactions on Industry Applications*, 45(5), 1879-1887.

[11] Yan X, Venkataramanan G, Flannery PS, Wang Y, Dong Q, Zhang B. Voltage-Sag Tolerance of DFIG Wind Turbine With A Series Grid Side Passive-Impedance Network. *IEEE Transactions on Energy Conversion*, 25(4), 1048-1056, 2010.

[12] Abdel-Baqi O, Nasiri A. Series Voltage Compensation for DFIG Wind Turbine Low-Voltage Ride-Through Solution. *IEEE Transactions on Energy conversion*, 26(1), 272-280, 2011.

[13] Zhu D, Zou X, Zhou S, Dong W, Kang Y, Jiabing HU. Feedforward Current References Control for DFIG-Based Wind Turbine to Improve Transient Control Performance During Grid Faults. *IEEE Transactions on Energy Conversion*, 33, 670-681, 2018.

[14] Amalorpavaraj RAJ, Kaliannan P, Padmanaban S, Subramaniam U, Ramachandaramurthy VK. Improved Fault Ride Through Capability in DFIG Based Wind Turbines Using Dynamic Voltage Restorer With Combined Feed-Forward and Feed-Back Control. *IEEE Access*, 5, 20494-20503, 2017.

[15] Sun D, Wang X, Nian H, Zhu ZQ. A Sliding-Mode Direct Power Control Strategy for DFIG Under Both Balanced and Unbalanced Grid Conditions Using Extended Active Power. *IEEE Transactions on Power Electronics*, 33(2), 1313-1322, 2018.

[16] Liu Y, Wang Z, Xiong L, Wang J, Jiang X, Bai G, Liu S. DFIG Wind Turbine Sliding Mode Control With Exponential Reaching Law Under Variable Wind Speed. *International Journal of Electrical Power & Energy Systems*, 96, 253-260, 2018.

[17] Döşoğlu MK. Enhancement of SDRU and RCC for Low Voltage Ride Through Capability in DFIG Based Wind Farm. *Electrical Engineering*, 99(2), 673-683, 2017.

[18] Shahbazi M, Poure P, Saadate S. Real-time Power Switch Fault Diagnosis and Fault-Tolerant Operation in A DFIG-Based Wind Energy System. *Renewable Energy*, 116, 209-218, 2018.

[19] Alsmadi YM, Xu L, Blaabjerg F, Ortega AP, Abdelaziz AY, Wang A, Albataineh Z. Detailed Investigation and Performance Improvement of the Dynamic Behavior of Grid-Connected DFIG-Based Wind Turbines under LVRT Conditions. *IEEE Transactions on Industry Applications*, 54(5), 4795-4812, 2018.

[20] Mojallal A, Lotfifard S. DFIG Wind Generators Fault Diagnosis Considering Parameter and Measurement Uncertainties. *IEEE Transactions on Sustainable Energy*, 9(2), 792-804, 2018.

[21] Gounder YK, Nanjundappan D, Boominathan V, Enhancement of Transient Stability of Distribution System with SCIG and DFIG Based Wind Farms Using STATCOM. *IET Renewable Power Generation*, 10(8), 1171-1180, 2016.

[22] Kumar NS, Gokulakrishnan J. Impact of FACTS Controllers on The Stability of Power Systems Connected with Doubly Fed Induction Generators. *International Journal of Electrical Power & Energy Systems*, 33(5), 1172-1184, 2011.

[23] Döşoğlu MK, Öztürk A. Investigation of Different Load Changes In Wind Farm by using FACTS Devices. *Advances in Engineering Software*, 45(1), 292-300, 2012.

[24] Mohanty A, Viswavandya M, Ray PK, Patra S. Stability Analysis and Reactive Power Compensation Issue in A Microgrid with A DFIG Based WECS. *International Journal of Electrical Power & Energy Systems*, 62, 753-762, 2014.

[25] Hossain MJ, Saha TK, Mithulananthan N, Pota HR. Control Strategies for Augmenting LVRT Capability of DFIGs in Interconnected Power Systems. *IEEE Transactions on Industrial Electronics*, 60(6), 2510-2522, 2012.

[26] Xiao S, Yang G, Zhou H, Geng H. An LVRT Control Strategy Based on Flux Linkage Tracking for DFIG-Based WECS. *IEEE Transactions on Industrial Electronics*, 60(7), 2820-2832, 2012.

[27] Rahimi M, Parniani M. Efficient Control Scheme of Wind Turbines with Doubly Fed İnduction Generators for Low-Voltage Ride-Through Capability Enhancement. *IET Renewable Power Generation*, 4(3), 242-252, 2010.

[28] Mendes VF, de Sousa CV, Silva SR, Rabelo BC, Hofmann W. Modeling and Ride-Through Control of Doubly Fed İnduction Generators During Symmetrical Voltage Sags. *IEEE Transactions on Energy Conversion*, 26(4), 1161-1171, 2011.

[29] López J, Gubía E, Olea E, Ruiz J, Marroyo L. Ride Through of Wind Turbines with Doubly Fed İnduction Generator Under Symmetrical Voltage Dips. *IEEE Transactions on Industrial Electronics*, 56(10), 4246-4254, 2009.

[30] Döşoğlu MK, Güvenç U, Sönmez Y, Yılmaz C. Enhancement of Demagnetization Control for Low-Voltage Ride-Through Capability in DFIG-Based Wind Farm. *Electrical Engineering*, 100, 491-498, 2018.

[31] Döşoğlu MK. A New Approach for Low Voltage Ride Through Capability in DFIG Based Wind Farm.

International Journal of Electrical Power Energy Systems, 83, 251-258, 2016.

[32] Mohammadi J, Afsharnia S, Vaez-Zadeh S, Farhangi S, Improved Fault Ride Through Strategy for Doubly Fed Induction Generator Based Wind Turbines Under Both Symmetrical and Asymmetrical Grid Faults. *IET Renewable Power Generation*, 10(8), 1114-1122, 2016.

[33] Mohammadi J, Afsharnia S, Ebrahimzadeh E, Blaabjerg F. An Enhanced LVRT Scheme for DFIG-based WECSs under Both Balanced and Unbalanced Grid Voltage Sags. *Electric Power Components and Systems*, 45(11), 1242-1252, 2017.

[34] Mohammadi J, Afsharnia S, Vaez-Zadeh S. Efficient Fault-Ride-Through Control Strategy of DFIG-Based Wind Turbines During The Grid Faults. *Energy Conversion and Management*, 78, 88-95, 2014.

[35] Krause PC, Wasynczuk O, Sudhoff SD. *Analysis of Electric Machinery*. McGraw-Hill Education, New York, USA, 1986.

[36] Döşoğlu MK. Nonlinear Dynamic Modeling for Fault Ride-Through Capability of DFIG-Based Wind Farm. *Nonlinear Dynamics*, 89(4), 2683-2694, 2017.

[37] Ekanayake JB, Holdsworth L, Jenkins N. Comparison of 5th Order and 3rd Order Machine Models for Doubly Fed İnduction Generator (DFIG) Wind Turbines. *Electric Power Systems Research*, 67(3), 207-215, 2003.

[38] Slootweg JG, Polinder H, Kling WL. Dynamic modelling of a wind turbine with doubly fed induction generator. *2001 Power Engineering Society Summer Meeting. Conference Proceedings*, Vancouver, 15-19 July 2001.

[39] Döşoğlu MK, Arsoy AB. Enhancement of A Reduced Order Doubly Fed Induction Generator Model for Wind Farm Transient Stability Analyses. *Turkish Journal of Electrical Engineering & Computer Sciences*, 24(4), 2124-2134, 2016.